

# AN ALTERNATIVE METHOD FOR CHARACTERIZATION AND COMPARISON OF PLANT ROOT SHAPES

A thesis submitted to the  
College of Graduate and Postdoctoral Studies  
in partial fulfillment of the requirements  
for the degree of Master of Science  
in the Department of School of Environment and Sustainability  
University of Saskatchewan  
Saskatoon

By  
Yujie Pei

©Yujie Pei, Month/Year. All rights reserved.

# CONTENTS

<b>1</b>	<b>Existing Morphological Descriptors for Root Systems</b>	<b>4</b>
<b>2</b>	<b>An Alternative Mathematical Method for Shape Description</b>	<b>5</b>
2.1	Kac's Idea: Can One Hear the Shape of a Drum? [5] . . . . .	6
2.1.1	Interpretations of Kac's Problem . . . . .	6
2.1.2	Problem Statement . . . . .	6
2.1.3	Summarize the Results of Kac's Idea . . . . .	6
2.1.4	Conclusion . . . . .	7
2.1.4.1	Advantages . . . . .	7
2.1.4.2	Limitations . . . . .	7
<b>3</b>	<b>LRWs in Artificial Images</b>	<b>8</b>
3.1	Circle and Rectangle . . . . .	9
3.1.1	Output Analysis . . . . .	9
3.1.2	Conclusion . . . . .	9
3.2	Complicated Branching Structures . . . . .	12
3.2.1	Output Analysis of $S(n)$ . . . . .	12
3.2.1.1	$S(d)$ . . . . .	15
3.2.1.2	$S(R)$ . . . . .	22
3.2.2	Conclusion . . . . .	23
<b>4</b>	<b>LRWs in Real Root Images</b>	<b>24</b>
<b>5</b>	<b>Conclusion</b>	<b>25</b>
<b>6</b>	<b>Future Work</b>	<b>26</b>
<b>Appendix A</b>	<b>Numerical Methods for Solving Parabolic Partial Differential Equations</b>	<b>27</b>
A.1	Introduction . . . . .	28
A.2	Summary of Commonly Used Numerical Techniques . . . . .	28
A.3	Limitation in Practice . . . . .	28
<b>Appendix B</b>	<b>Method Validation in Annulus</b>	<b>29</b>
B.1	Analytical Results . . . . .	30
B.1.1	Shape Description . . . . .	30

B.1.2	Solving Initial-Boundary Value Problem (IBVP) . . . . .	30
B.1.2.1	Methods . . . . .	30
B.1.2.2	Mathematical Equations . . . . .	30
B.1.2.3	Heat Content Calculation . . . . .	30
B.2	Numerical Approximation . . . . .	30
B.2.1	Eigenvalues $\lambda_{0,n}$ . . . . .	30
B.2.2	Approximation of $u(\hat{r}, \theta, \tau)$ and $S(\tau)$ . . . . .	31
B.3	Comparison of Numerical and Analytical Results . . . . .	31
B.3.1	Sample Size Evaluation . . . . .	31
B.3.2	Comparison of $S(\tau)$ and $S(n)$ . . . . .	31
B.4	Conclusion . . . . .	31
<b>Appendix C Artificial Images</b>		<b>32</b>
C.1	Simple Shapes . . . . .	33
C.2	Complicated Branching Structures . . . . .	33
<b>References</b>		<b>36</b>

# EXISTING MORPHOLOGICAL DESCRIPTORS FOR ROOT SYSTEMS

# AN ALTERNATIVE MATHEMATICAL METHOD FOR SHAPE DE- SCRIPTION

## 2.1 Kac's Idea: Can One Hear the Shape of a Drum? [5]

### 2.1.1 Interpretations of Kac's Problem

- When the drum vibrates, one can hear the sound, which is composed of tones of various frequencies. How much can shape features be inferred from hearing a discrete spectrum of pure tones produced by a drum?
- If a complete sequence of eigenvalues of the Dirichlet problem for the Laplacian can be obtained precisely, will people determine the shape of a planar?

### 2.1.2 Problem Statement

- Consider a simply connected membrane  $\Omega$  in the Euclidean space bounded by a smooth convex curve  $\partial\Omega$  (e.g. a drum without any holes)
- Find function  $\phi$  on the closure of  $\Omega$ , which vanishes at the boundary  $\partial\Omega$ , and a number  $\lambda$  satisfying  $-\Delta\phi = \lambda\phi$ .
  - $\Delta$  is the Laplace operator. e.g.  $\Delta = \sum_{i=1}^n \frac{\partial^2}{\partial x_i^2}$  in Cartesian coordinate system.
  - If there exists a solution  $\phi \neq 0$ , the corresponding  $\lambda$  is defined as a Dirichlet eigenvalue.
  - For each domain  $\Omega$ , there has a sequence of eigenvalues  $\lambda_1, \lambda_2, \lambda_3, \dots$  corresponding to a set of eigenfunction  $\phi_1, \phi_2, \phi_3, \dots$
  - $\phi_k$  form an orthonormal basis of  $L^2(\Omega)$  of real valued eigenfunctions; the corresponding discrete Dirichlet eigenvalues are positive ( $\lambda_k \in \mathbb{R}^+$ ).
- An important function [4]:

$$h(t) = \sum_{k=1}^{\infty} e^{-\lambda_k t} \quad (2.1)$$

- It is a Dirichlet series.
- It is called the spectral function or the heat trace.
- It is smooth and converges for every  $t > 0$ .

### 2.1.3 Summarize the Results of Kac's Idea

$$h(t) = \sum_{k=1}^{\infty} e^{-\lambda_k t} \sim \frac{|\Omega|}{2\pi t} - \frac{L}{4} \frac{1}{\sqrt{2\pi t}} + \frac{1}{6} \quad (2.2)$$

- As  $t \rightarrow 0^+$ , the leading terms of the asymptotic expansion of  $h(t)$  imply the geometrical attributes of  $\Omega$

- the total area
  - the perimeter
  - the curvature
- If the domain  $\Omega$  has the polygonal boundary, the third term shows in the information about the interior angles of the polygon [4].

## 2.1.4 Conclusion

### 2.1.4.1 Advantages

- Kac proposed a novel analytical mathematical method for the shape description without using measuring tools, e.g. rulers.
- Other mathematicians extended Kac's idea in exploring the geometrical information of more complex domains with various boundary conditions [6][3][2] [9][7].

### 2.1.4.2 Limitations

- It is only available for the convex domain, which has a smooth or piecewise smooth boundary.
- Except in very few cases (i.e. rectangular, disk, certain triangles), the complete sequence of eigenvalues  $\lambda_k$  can not be calculated [4].
- Only the first few terms in the asymptotic expansion of  $h(t)$  are explicitly available.

# LRWs IN ARTIFICIAL IMAGES



	test_statistic	p
Logrank	137.23	0.0
Tarone-Ware	134.31	0.0
Gehan-Breslow	123.83	0.0
Fleming-Harrington	123.83	0.0

**Table 3.1:** Survival functions for circle and rectangle are statistically different since p values equal zeros.

The fixed-time step Monte Carlo simulation, LRWs, has been validated in the annulus in Appendix B by comparing the analytical and numerical survival function. The further validation of LRWs is to distinguish the geometries and explore their structural features from both short and long time behaviours of the survival function.

### 3.1 Circle and Rectangle

Given two simple convex shapes with the same area, circle and rectangle, we are interested in how and whether their corresponding survival curves differ from each other. For the equal-area geometries, rectangle and circle, Eq. 2.2 indicates that the survival function of the former decays faster than the latter as the time approaches zero.

The preliminary step of testing the research hypothesis is to generate two black-and-white images with the same dimensions as shown in Fig. C.1. In the binary images, circle and rectangle have an equal number of white pixels. For simplicity, the centroid of shapes located at the center of the image. Then, simulating LRWs in the images and estimating survival functions by Kaplan-Meier estimator.

#### 3.1.1 Output Analysis

The differences between survival functions for the circle and rectangle are not visible. Moreover, the approximate 95% confidence intervals of the survival functions overlap. In this case, non-parametric statistical tests can be used to compare entire survival distributions and assess their dissimilarities. The logrank test has maximum power if the proportional hazards assumption is satisfied.

#### 3.1.2 Conclusion

Although the proportional hazard assumption test is failed as shown in Fig. ??, the weighted logrank tests indicate that the null hypothesis should be rejected. In conclusion, LRWs is an alternative tool to quantify and distinguish the geometries in the 2– dimensional image without measuring the predefined shape descriptors.

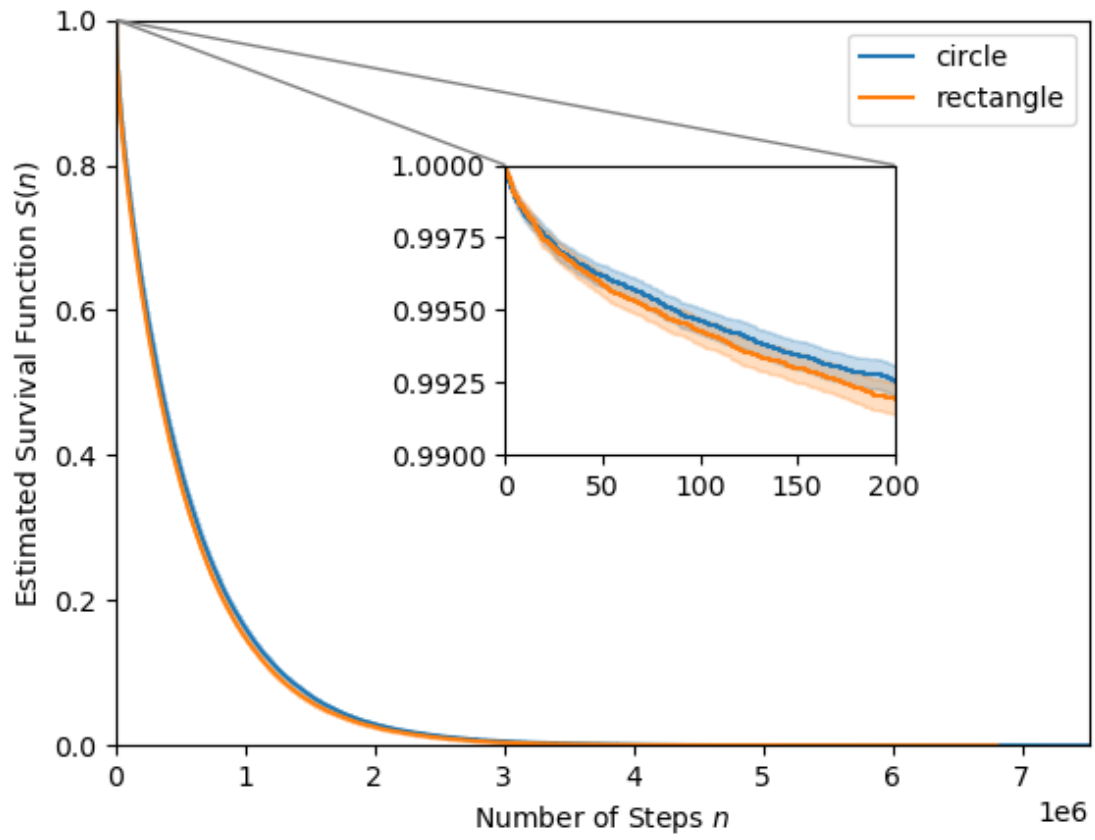


**Figure 3.1:** In the inset plot, the decay rate of the survival function for the rectangle is slightly larger than for the circle, which coincides with the theoretical result.

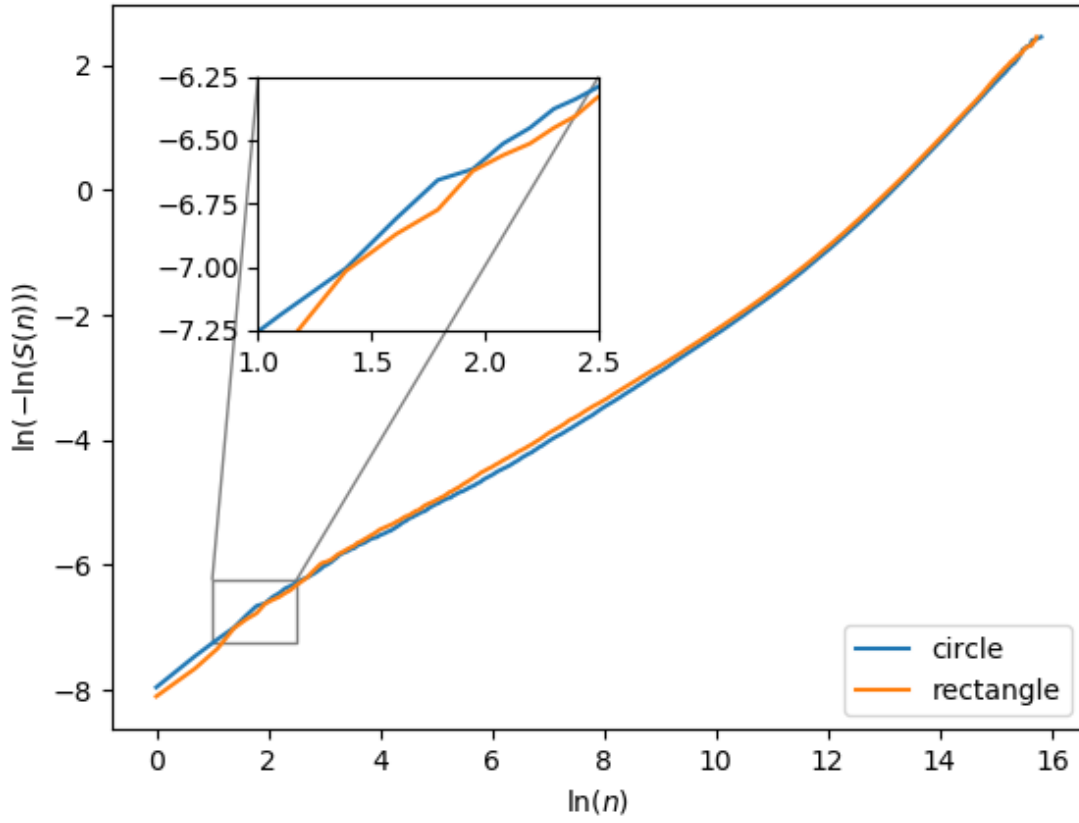


**Figure 3.2:** This is a graphical method for checking proportionality by looking for parallelism. As shown in the inset plot, two curves cross at some points and their shapes vary over time. Moreover,  $p < 0.05$  in the non-proportional test. Thus, the survival data for circle and rectangle does not satisfy the proportional hazard assumption.

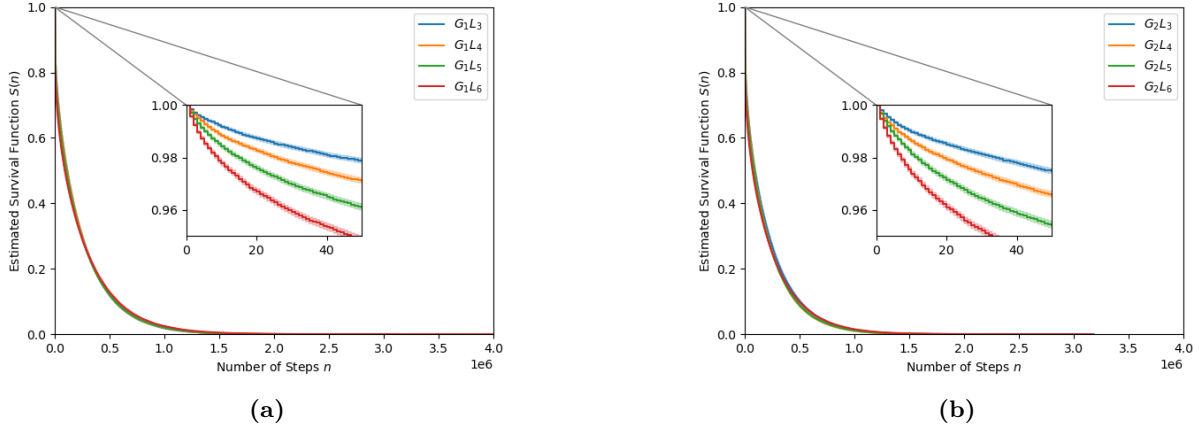


**Figure 3.3:** (a) and (b) are survival functions for branching structures in  $G_1$  and  $G_2$ , respectively.  $n$  is the number of steps taken by the particle from the initial to the stop pixel in LRWs.

## 3.2 Complicated Branching Structures

In the preceding section, the research hypothesis has been tested by the comparison of simple shapes. In the preceding section, the research hypothesis has been tested by the comparison of simple shapes. More complex branching structures, as shown in Fig. C.2 and Fig. C.3, are produced in this section for further test and understanding of the survival curve. The branching structures in the images are equal-area and vertically symmetric, but the template in  $G_1$  is shorter and narrower than in  $G_2$ . In  $G_i$ ,  $i = 1, 2$ , the larger number of iterations  $j$ , the more complicated structures  $L_j$ ,  $j = 3, 4, 5, 6$ , with more nodes.

### 3.2.1 Output Analysis of $S(n)$

The inset plot in Fig. 3.3 shows that the decay rates of  $S(n)$  for  $L_j$ ,  $j = 3, \dots, 6$ , are significantly distinct. The graphical representation is consistent with the analytical result since bigger  $j$  results in the larger perimeter of the branching structure. Some weighted log-rank tests can be utilized to detect the early or late differences between the pairwise overlapping or crossing survival curves. In Table 3.2 and Table 3.3, TW is the abbreviation for Tarone-Ware test, GB is for Gehan-Breslow test, and FH is for Fleming-Harrington test. However, p values in the tables are not too informative, and the log-rank test under conditions of non-proportional hazards leads to misleading results.

Distance measures are alternative methodologies for quantifying the discrepancy between survival functions. It is assumed that  $\hat{S}_1(t)$  and  $\hat{S}_2(t)$  are the Kaplan-Meier estimators of the survival functions for random variable  $T_1 > 0$  and  $T_2 > 0$ , respectively. Let  $(\tau_j)_{j=1,2,\dots,N}$  are distinct increasing observed times when the event of interest take place.

In the vector space, the distance between  $\hat{S}_1(t)$  and  $\hat{S}_2(t)$  can be defined as the  $L_p$  norm of their difference,  $1 \leq p \leq \infty$ , where

		p			
		Log-rank	TW	GB	FH
$G_1 \ L_3$	$G_1 \ L_4$	0.4393	0.0285	0.0005	0.0005
	$G_1 \ L_5$	0.0	0.0	0.0	0.0
	$G_1 \ L_6$	0.0	0.0	0.0	0.0
$G_1 \ L_4$	$G_1 \ L_5$	0.0007	0.0	0.0	0.0
	$G_1 \ L_6$	0.0002	0.0	0.0	0.0
$G_1 \ L_5$	$G_1 \ L_6$	0.7223	0.0	0.0	0.0

**Table 3.2:** The differences between the pairwise survival functions for branching objects in  $G_1$  are statistically significant.

		p			
		Log-rank	TW	GB	FH
$G_2 \ L_3$	$G_2 \ L_4$	0.0	0.0	0.0	0.0
	$G_2 \ L_5$	0.0	0.0	0.0	0.0
	$G_2 \ L_6$	0.0	0.0	0.0	0.0
$G_2 \ L_4$	$G_2 \ L_5$	0.0016	0.0	0.0	0.0
	$G_2 \ L_6$	0.0004	0.0	0.0	0.0
$G_2 \ L_5$	$G_2 \ L_6$	0.7199	0.0	0.0	0.0

**Table 3.3:** As mentioned before, the log-rank test will lose power if the proportional hazard assumption is violated. Except for the log-rank test, other statistical tests' results tell us that the pairwise survival functions are statistically different.

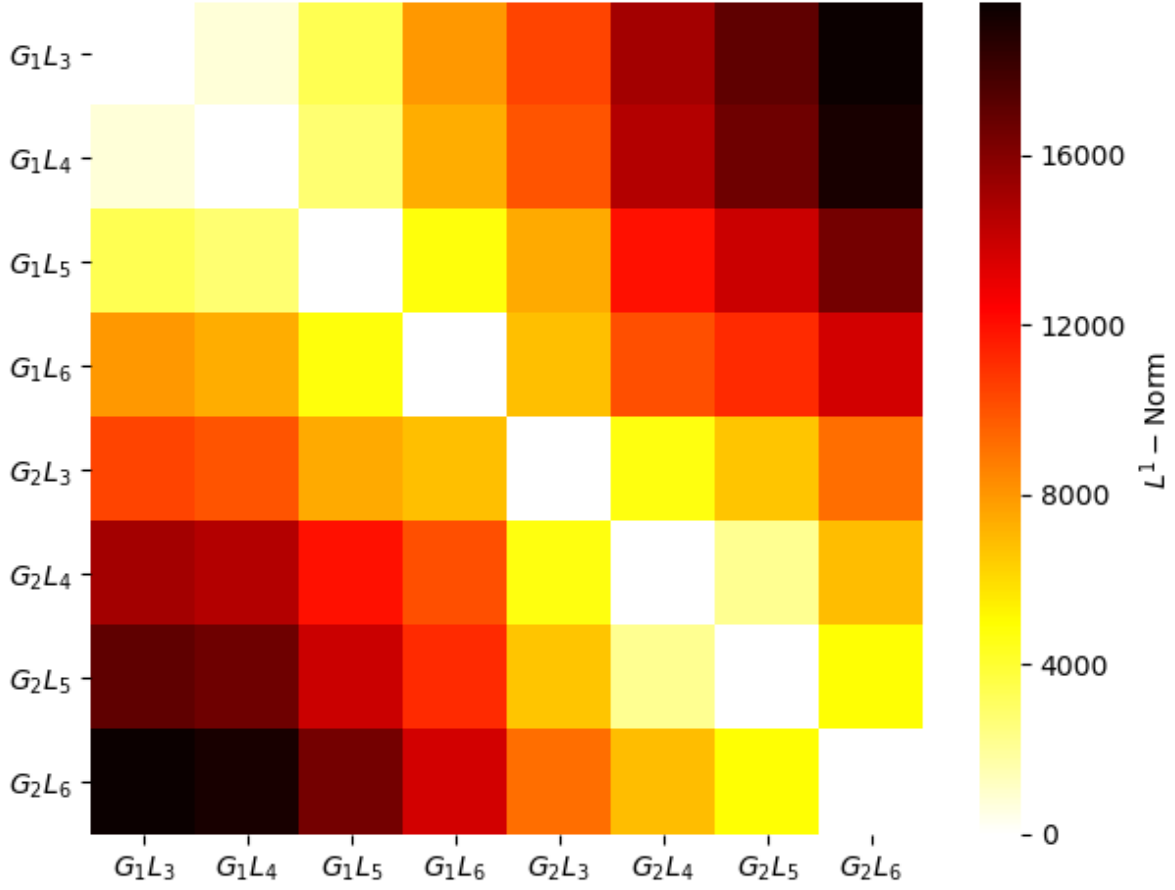


**Figure 3.4:** The distance matrix of pairwise survival functions for artificial images is visualized by a heat map, where  $L^1$  norm is the distance metric.

$$\begin{aligned}
 d_p(\hat{S}_1(t), \hat{S}_2(t)) &= \|\hat{S}_1(t) - \hat{S}_2(t)\|_p \\
 &= \left( \sum_{j=1}^N |\hat{S}_1(\tau_j) - \hat{S}_2(\tau_j)|^p \right)^{\frac{1}{p}} \\
 &= \left( \sum_{j=1}^N |P(T_1 > \tau_j) - P(T_2 > \tau_j)|^p \right)^{\frac{1}{p}}
 \end{aligned} \tag{3.1}$$

As shown in Fig. 3.4, when  $p$  equals 1 in Eq. 3.1, the dissimilarities between each pair of survival functions are measured by  $d_1$  and depicted by color. The cells on the main diagonal are white because of the identity of indiscernibles. The colors of off-diagonal cells are symmetric, and the darker indicates more significant dissimilarities between survival functions. In other words, the color of cells implies the shape variation of branching structures in the artificial images.

The top left and bottom right square patterns are the in-group shape comparison, while the top right and bottom left square patterns are the between-group shape comparison.

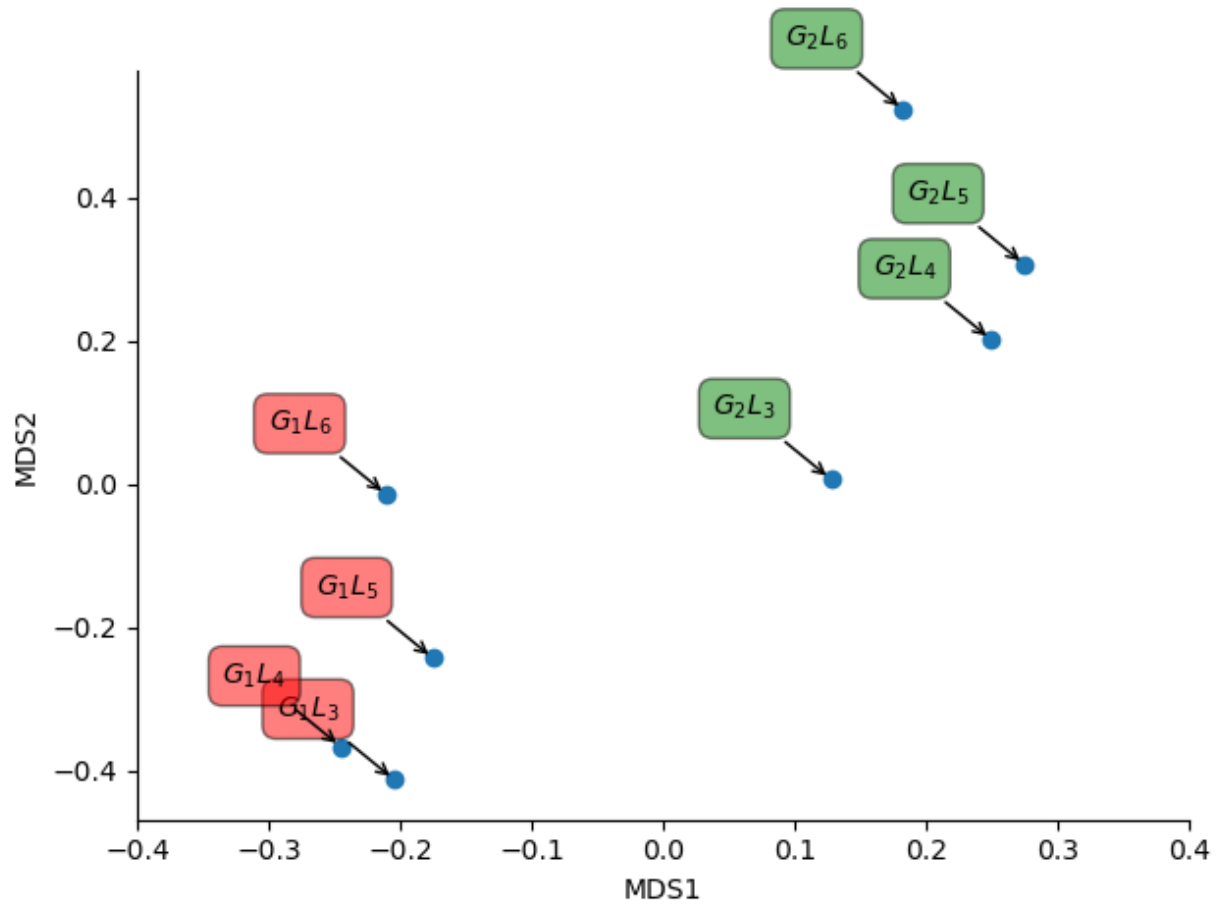


Figure 3.5

### 3.2.1.1 $S(d)$

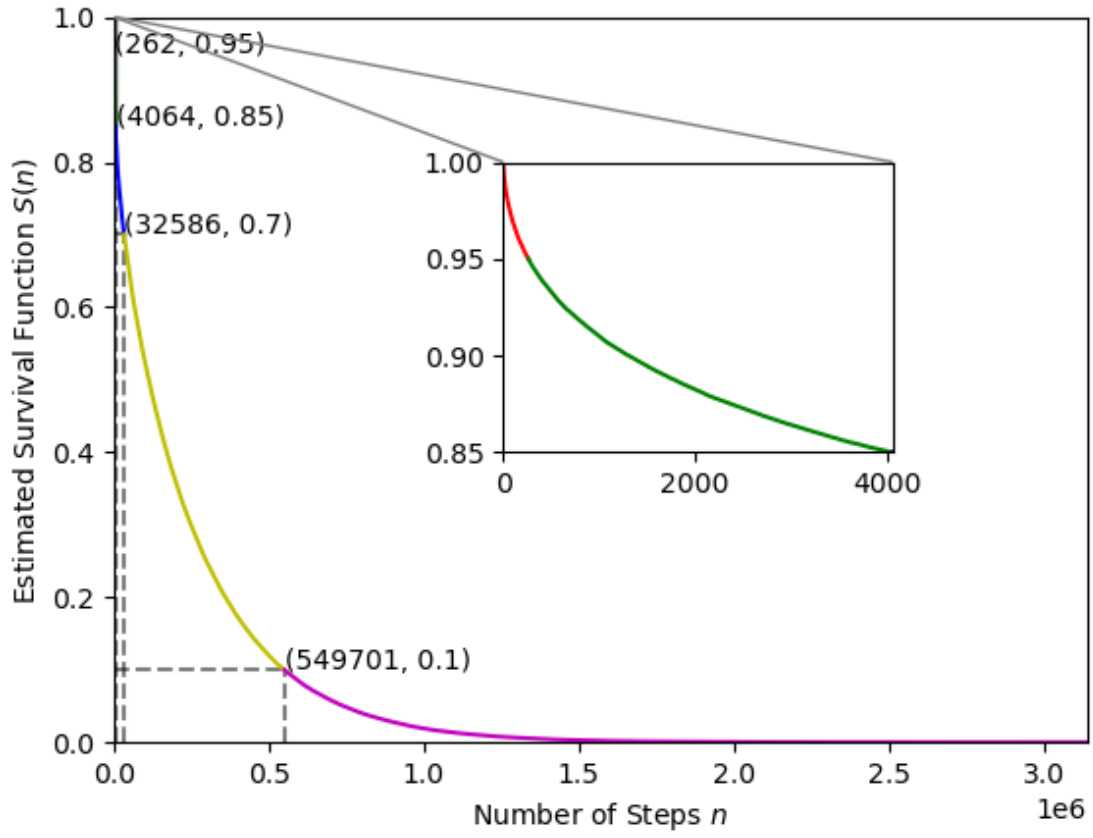


Figure 3.6

		p			
		Logrank	TW	GB	FH
$G_1 L_3$	$G_1 L_4$	0.0	0.0	0.0	0.0
	$G_1 L_5$	0.0	0.0	0.0	0.0
	$G_1 L_6$	0.0	0.0	0.0	0.0
$G_1 L_4$	$G_1 L_5$	0.0072	0.0	0.0	0.0
	$G_1 L_6$	0.0003	0.0	0.0	0.0
$G_1 L_5$	$G_1 L_6$	0.2883	0.0	0.0	0.0

Table 3.4



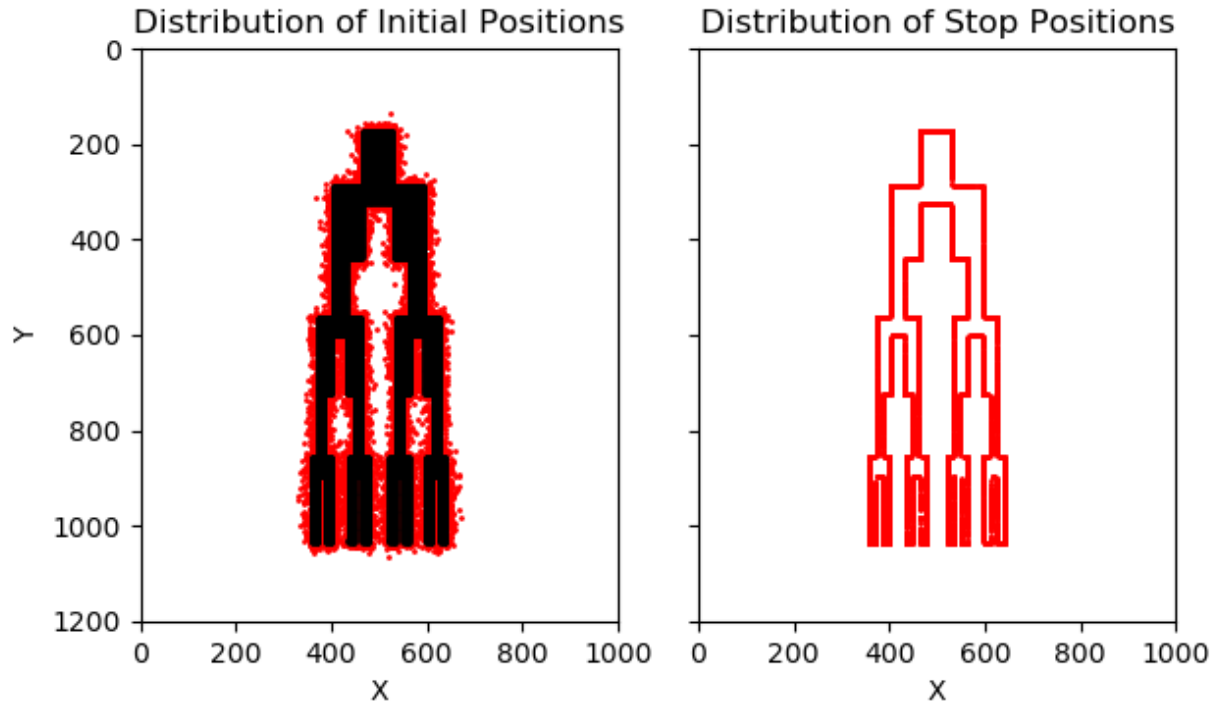


Figure 3.7

		p			
		Logrank	TW	GB	FH
$G_2 L_3$	$G_2 L_4$	0.0	0.0	0.0	0.0
	$G_2 L_5$	0.0	0.0	0.0	0.0
	$G_2 L_6$	0.0	0.0	0.0	0.0
$G_2 L_4$	$G_2 L_5$	0.0001	0.0	0.0	0.0
	$G_2 L_6$	0.0015	0.0	0.0	0.0
$G_2 L_5$	$G_2 L_6$	0.7019	0.0	0.0	0.0

Table 3.5

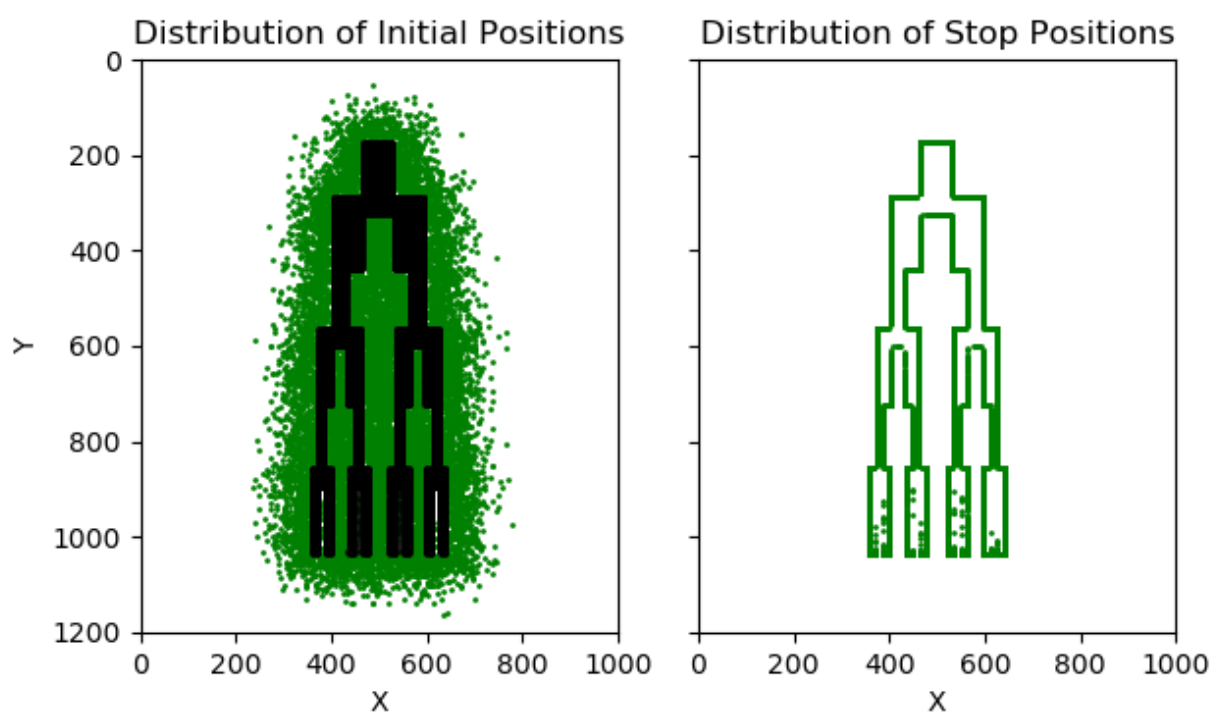


Figure 3.8

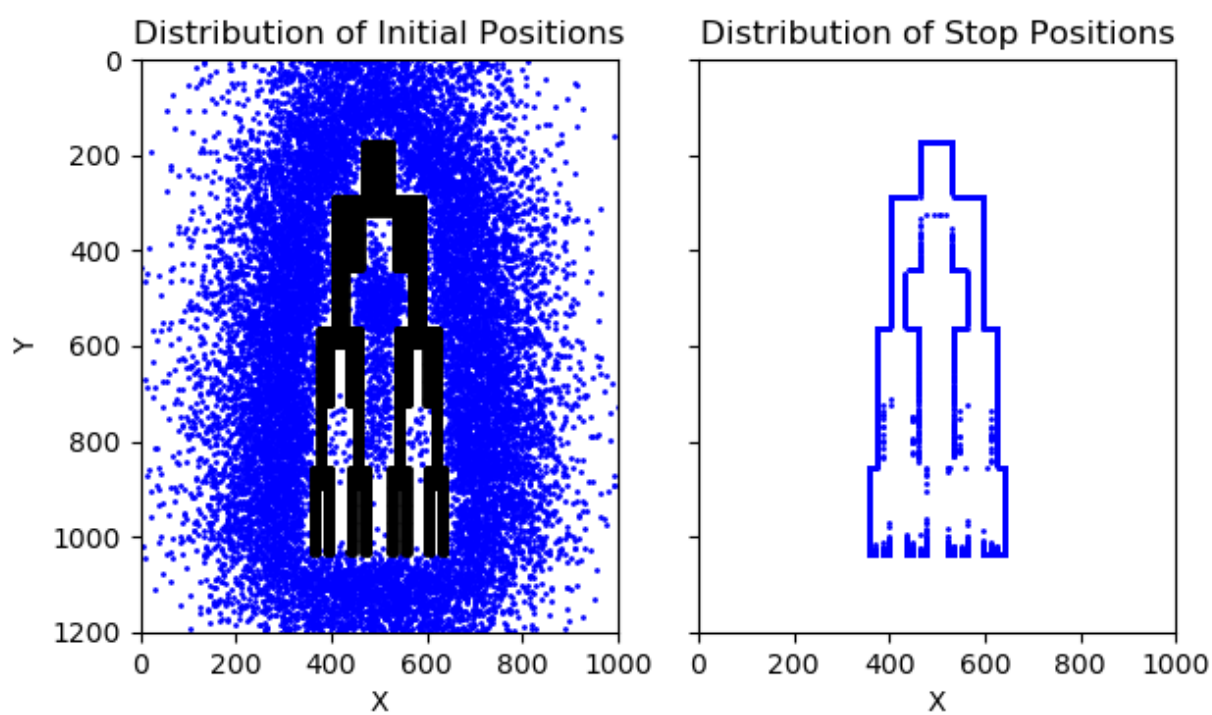


Figure 3.9

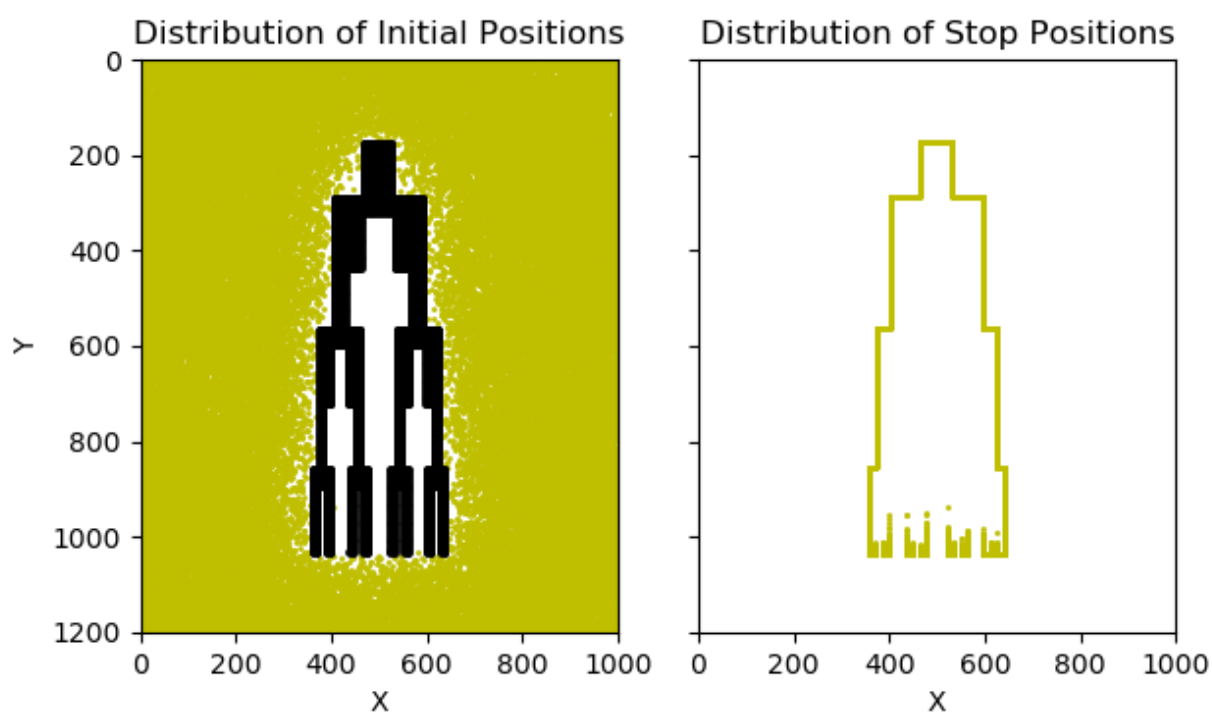


Figure 3.10

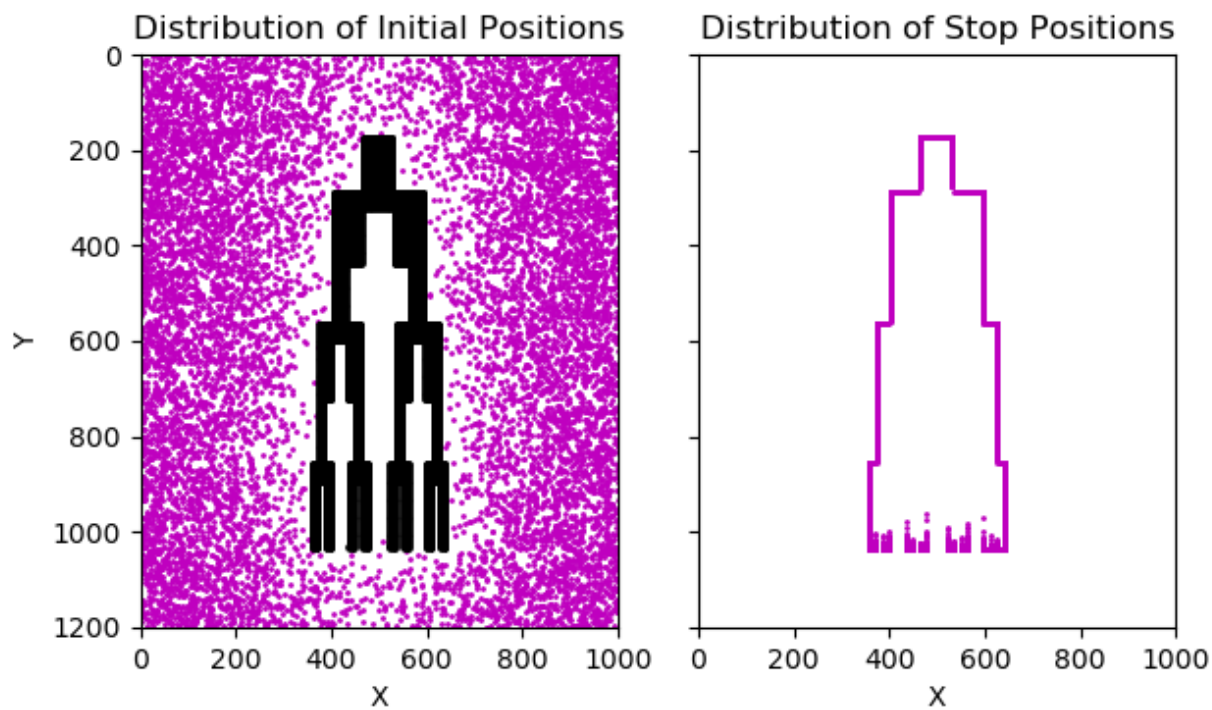


Figure 3.11

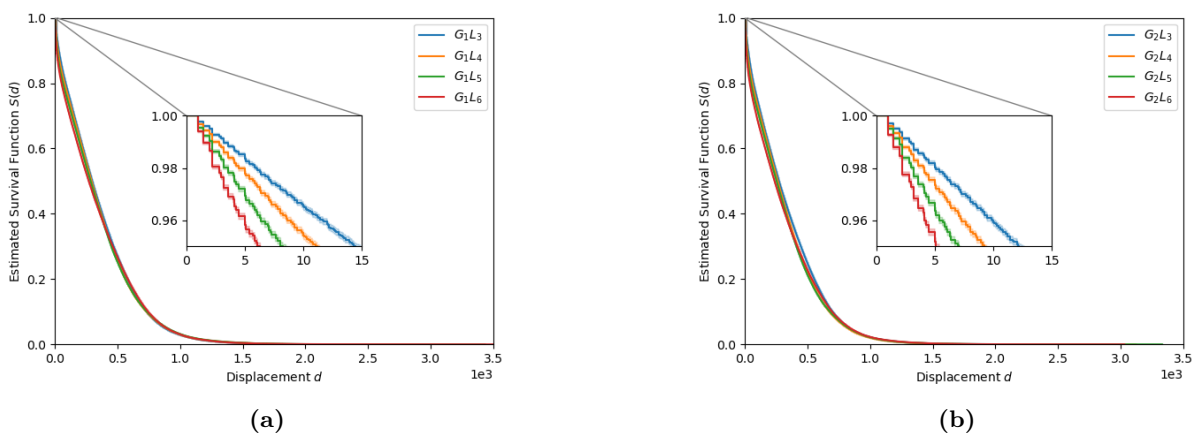
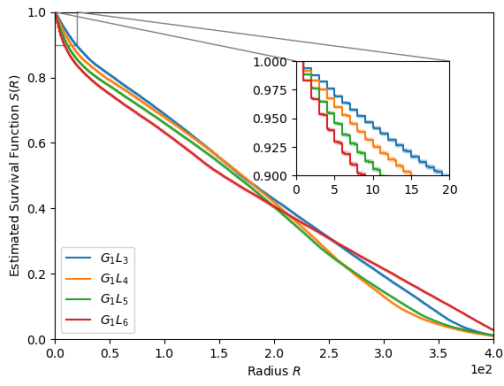
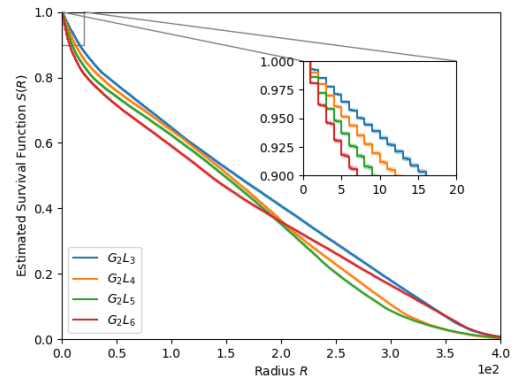


Figure 3.12



(a)



(b)

Figure 3.13

		p			
		Logrank	TW	GB	FH
$G_1 L_3$	$G_1 L_4$	0.0	0.0	0.0	0.0
	$G_1 L_5$	0.0	0.0	0.0	0.0
	$G_1 L_6$	0.0	0.0	0.0	0.0
$G_1 L_4$	$G_1 L_5$	0.1773	0.0	0.0	0.0
	$G_1 L_6$	0.0	0.0	0.0	0.0
$G_1 L_5$	$G_1 L_6$	0.0	0.0	0.0	0.0

Table 3.6

### 3.2.1.2 $S(R)$

		p			
		Logrank	TW	GB	FH
$G_2 \ L_3$	$G_2 \ L_4$	0.0	0.0	0.0	0.0
	$G_2 \ L_5$	0.0	0.0	0.0	0.0
	$G_2 \ L_6$	0.0	0.0	0.0	0.0
$G_2 \ L_4$	$G_2 \ L_5$	0.0	0.0	0.0	0.0
	$G_2 \ L_6$	0.0	0.0	0.0	0.0
$G_2 \ L_5$	$G_2 \ L_6$	0.0	0.0	0.0253	0.0253

**Table 3.7**

### 3.2.2 Conclusion

- In a short time, the survival function of rectangle decays faster than the circle, which conforms to the analytical results.
- The differences of estimated survival functions between circle and rectangle are statistically significant, which coincides with the real shape dissimilarities.
- Within a same group, when  $t$  is small, the more branching the object is, the faster the survival function decays.
- Within a same group, the pairwise survival functions are statistically different.
- The corresponding target structures in  $G_1$  and  $G_3$  are invariant shapes under translation since their survival function are not statistically different. In other words, periodic boundary conditions of the image can eliminate the effect of the locations.
- LRWs can describe and classify the geometries, their spatial configurations, and the unoccupied area in the image.

# LRWS IN REAL ROOT IMAGES



## CONCLUSION

## FUTURE WORK

APPENDIX A

NUMERICAL METHODS FOR SOLVING PARABOLIC PARTIAL  
DIFFERENTIAL EQUATIONS

**A.1 Introduction**

**A.2 Summary of Commonly Used Numerical Techniques**

**A.3 Limitation in Practice**

# APPENDIX B

## METHOD VALIDATION IN ANNULUS

## B.1 Analytical Results

### B.1.1 Shape Description

- Problem domain  $\Omega$ : the region bounded by two concentric circles
- Radius of the larger circle:  $b$
- Radius of the smaller circle:  $a$

### B.1.2 Solving Initial-Boundary Value Problem (IBVP)

#### B.1.2.1 Methods

- Dimensional Analysis: non-dimensional variables

$$\begin{aligned} - \mu &= \frac{b}{a} \\ - \tau &= \frac{t}{a^2} \\ - \hat{r} &= \frac{r}{a} \end{aligned}$$

- Method of separation of variables

#### B.1.2.2 Mathematical Equations

- Diffusion equation

$$u_\tau = (u_{\hat{r}\hat{r}} + \frac{1}{\hat{r}}u_{\hat{r}} + \frac{1}{\hat{r}^2}u_{\theta\theta}) \quad (\text{B.1})$$

- Uniform initial condition

$$u(\hat{r}, \theta, 0) = \frac{1}{|\Omega|} \quad (\text{B.2})$$

- Homogenous Dirichlet B.C.

$$u(1, \theta, \tau) = 0 \quad (\text{B.3})$$

- Homogenous Neumann B.C.

$$\hat{r}u'(\mu, \theta, \tau) = 0 \quad (\text{B.4})$$

#### B.1.2.3 Heat Content Calculation

$$S(\tau) = \int_0^{2\pi} d\theta \int_1^\mu \hat{r} d\hat{r} u(\hat{r}, \theta, \tau) \quad (\text{B.5})$$

## B.2 Numerical Approximation

### B.2.1 Eigenvalues $\lambda_{0,n}$

- Properties

- $\lambda_{0,n} \in \mathbb{R}^+$ , ( $n \in \mathbb{N}_+$ )
- Monotonicity and Periodicity

- Estimation

- $\lambda_{0,n} \in ((n-1)\pi, (n+1)\pi)$  [1]
- Bisection method [8]

### **B.2.2 Approximation of $u(\hat{r}, \theta, \tau)$ and $S(\tau)$**

- Direct summation
- Series acceleration methods

## **B.3 Comparison of Numerical and Analytical Results**

### **B.3.1 Sample Size Evaluation**

### **B.3.2 Comparison of $S(\tau)$ and $S(n)$**

## **B.4 Conclusion**

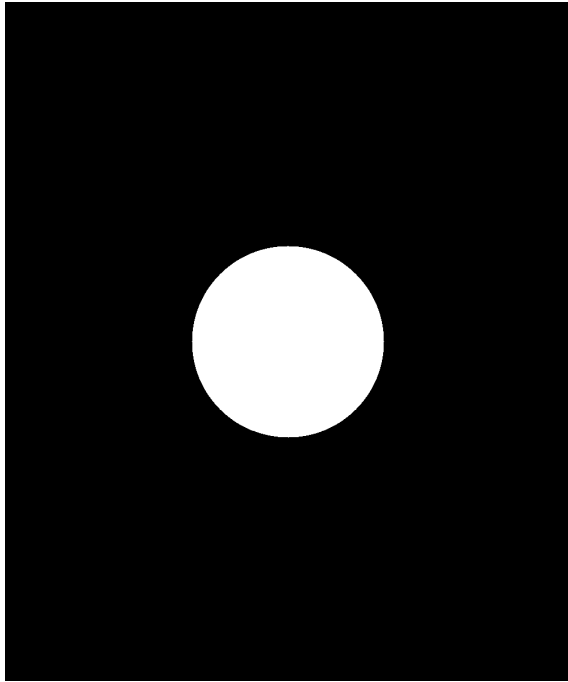
- The estimated survival function of LRWs is consistent with the analytical result.
- The number of particles in LRWs determined by DKW inequality is large enough to generate reproducible statistical results.

# APPENDIX C

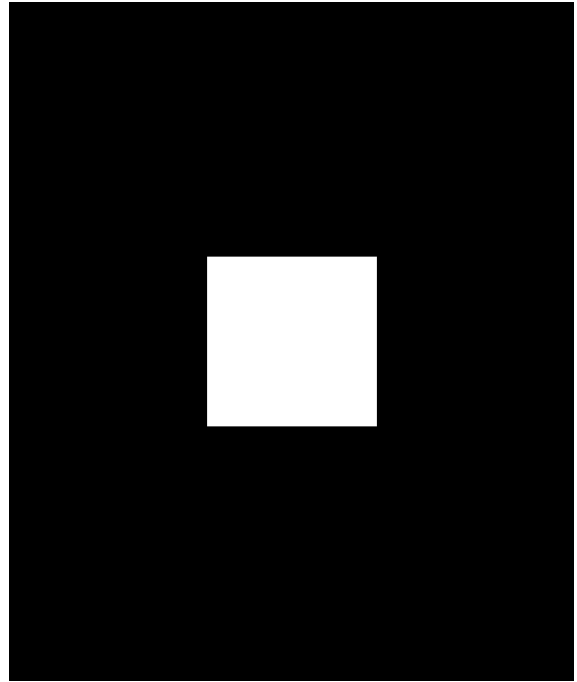
## ARTIFICIAL IMAGES



## C.1 Simple Shapes



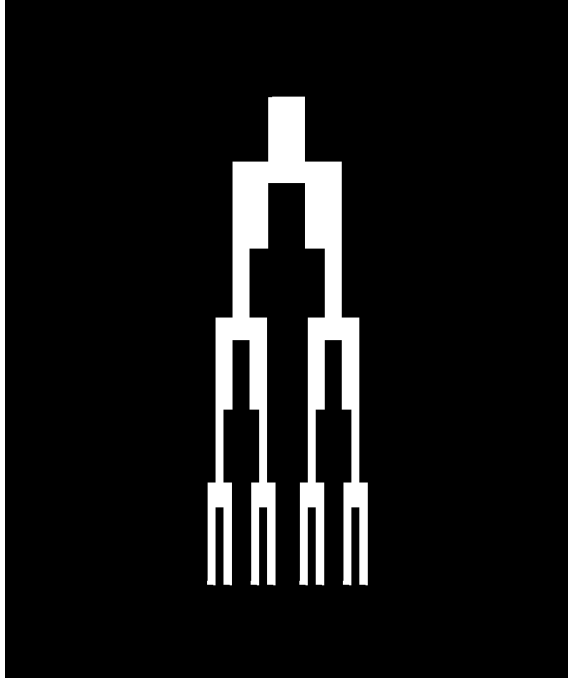
(a) Circle



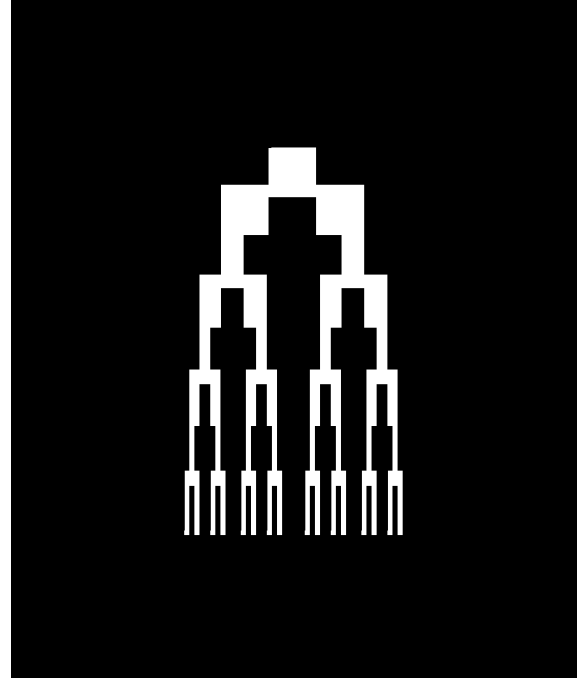
(b) Rectangle

**Figure C.1:** Each image size is 1200 by 1000 pixels with 90000 white pixels.

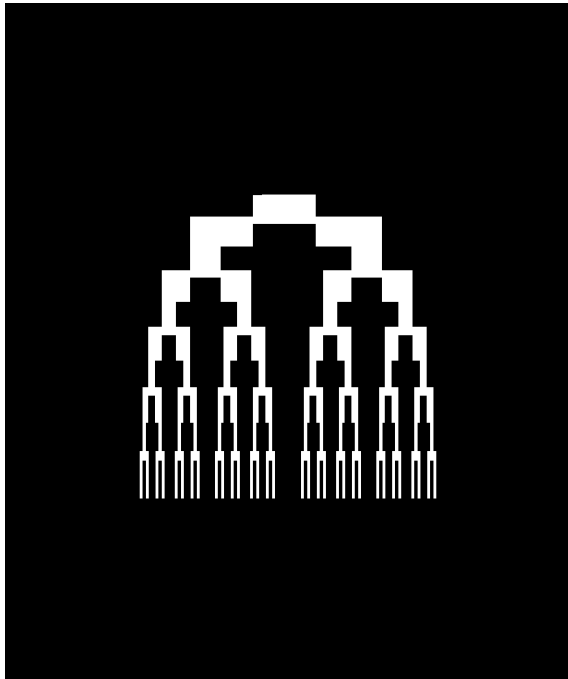
## C.2 Complicated Branching Structures



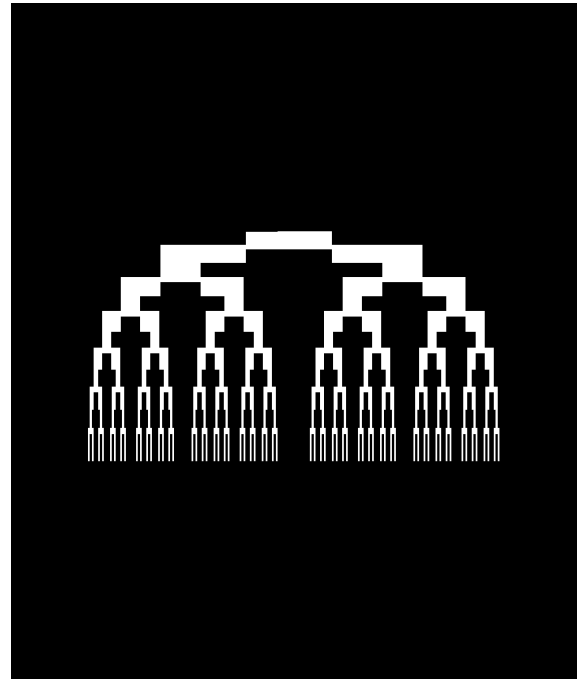
(a)  $G_1L_3$



(b)  $G_1L_4$

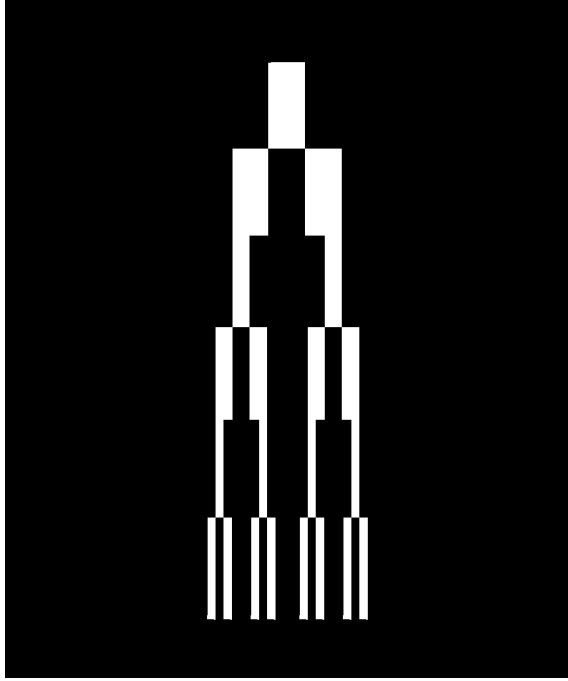


(c)  $G_1L_5$

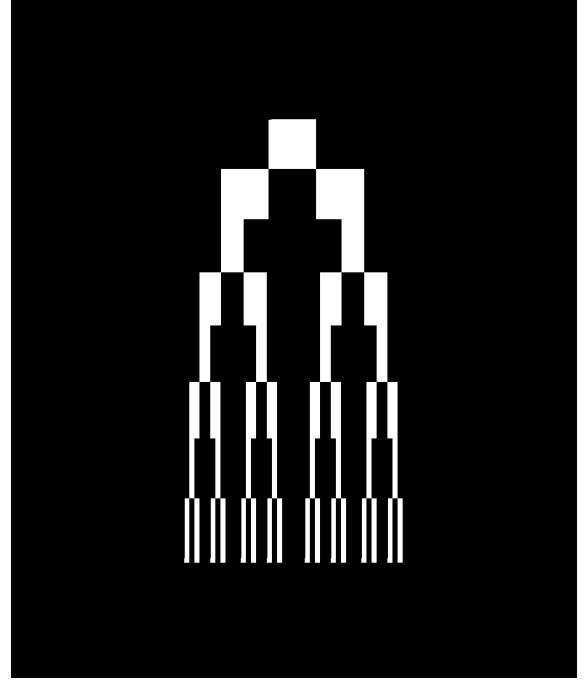


(d)  $G_1L_6$

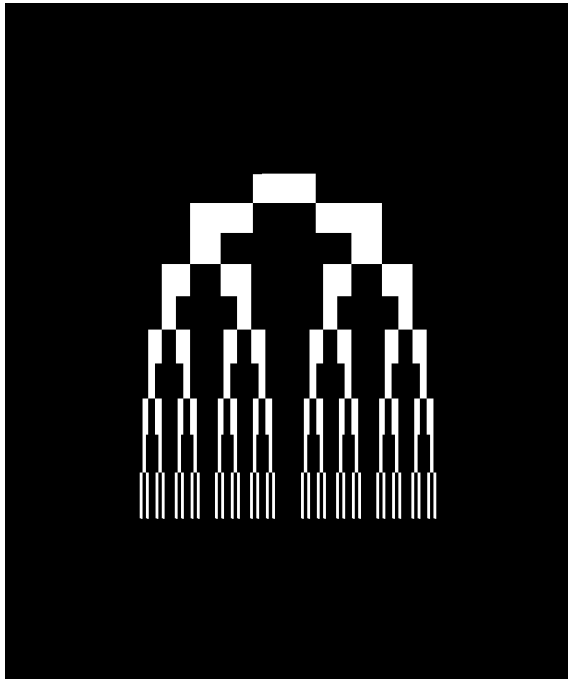
**Figure C.2:** In the group one, each image size is 1200 by 1000 pixels with 90000 white pixels.



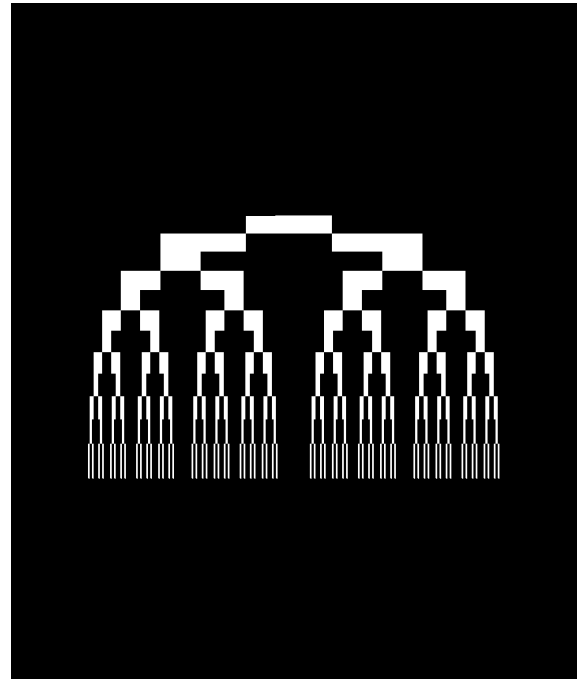
(a)  $G_2L_3$



(b)  $G_2L_4$



(c)  $G_2L_5$



(d)  $G_2L_6$

**Figure C.3:** In the group two, each image size is 1200 by 1000 pixels with 90000 white pixels.

# REFERENCES

- [1] *NIST Digital Library of Mathematical Functions*. <http://dlmf.nist.gov/>, Release 1.0.26 of 2020-03-15. F. W. J. Olver, A. B. Olde Daalhuis, D. W. Lozier, B. I. Schneider, R. F. Boisvert, C. W. Clark, B. R. Miller, B. V. Saunders, H. S. Cohl, and M. A. McClain, eds.
- [2] HPW Gottlieb. Hearing the shape of an annular drum. *The ANZIAM Journal*, 24(4):435–438, 1983.
- [3] HPW Gottlieb. Eigenvalues of the laplacian with neumann boundary conditions. *The ANZIAM Journal*, 26(3):293–309, 1985.
- [4] Daniel Grieser and Svenja Maronna. Hearing the shape of a triangle. *Notices of the American Mathematical Society*, 60(11):1440–1447, 2013.
- [5] Mark Kac. Can one hear the shape of a drum? *The American Mathematical Monthly*, 73(4P2):1–23, 1966.
- [6] Mohamed A Khabou, Lotfi Hermi, and Mohamed Ben Hadj Rhouma. Shape recognition using eigenvalues of the dirichlet laplacian. *Pattern Recognition*, 40(1):141–153, 2007.
- [7] BD Sleeman and EME Zayed. Trace formulae for the eigenvalues of the laplacian. *Zeitschrift für angewandte Mathematik und Physik*, 35(1):106–115, 1984.
- [8] Pauli Virtanen, Ralf Gommers, Travis E. Oliphant, Matt Haberland, Tyler Reddy, David Cournapeau, Evgeni Burovski, Pearu Peterson, Warren Weckesser, Jonathan Bright, Stéfan J. van der Walt, Matthew Brett, Joshua Wilson, K. Jarrod Millman, Nikolay Mayorov, Andrew R. J. Nelson, Eric Jones, Robert Kern, Eric Larson, CJ Carey, İlhan Polat, Yu Feng, Eric W. Moore, Jake Vand erPlas, Denis Laxalde, Josef Perktold, Robert Cimrman, Ian Henriksen, E. A. Quintero, Charles R Harris, Anne M. Archibald, Antônio H. Ribeiro, Fabian Pedregosa, Paul van Mulbregt, and SciPy 1.0 Contributors. SciPy 1.0: Fundamental Algorithms for Scientific Computing in Python. *Nature Methods*, 17:261–272, 2020.
- [9] EME Zayed. Heat equation for an arbitrary doubly-connected region in  $R^2$  with mixed boundary conditions. *Zeitschrift für angewandte Mathematik und Physik*, 40(3):339–355, 1989.